Determination of the size of the representative volume element for random quasi-brittle composites

Céline Pélissou, Jean Baccou, Yann Monerie, Frédéric Perales

Determination of the size of the representative volume element for random quasi-brittle composites

C. Pelissou [a,b], J. Baccou [a], Y. Monerie [a,b,*], F. Perales [a,b]

[a] Institut de Radioprotection et de Sûreté Nucléaire, B.P. 3, 13115 Saint-Paul-lez-Durance Cedex, France
[b] Laboratoire de Micromécanique et d'Intégrité des Structures, IRSN-CNRS-UMII, B.P. 3, 13115 Saint-Paul-lez-Durance Cedex, France

Keywords:
RVE size
Heterogeneous quasi-brittle material
Fracture energy
Periodic homogenization
Statistical approach

A B S T R A C T

A representative volume element (RVE) is related to the domain size of a microstructure providing a "good" statistical representation of typical material properties. The size of an RVE for the class of quasi-brittle random heterogeneous materials under dynamic loading is one of the major questions to be answered in this paper. A new statistical strategy is thus proposed for the RVE size determination. The microstructure illustrating the methodology of the RVE size determination is a metal matrix composite with randomly distributed aligned brittle inclusions: the hydrided Zircaloy constituting nuclear claddings. For a given volume fraction of inclusions, the periodic RVE size is found in the case of overall elastic properties and of overall fracture energy. In the latter case, the term "representative" is discussed since the fracture tends to localize. A correlation factor between the "elastic" RVE and the "fracture" RVE is discussed.

1. Introduction

A way to solve homogenization problems related to random media consists in using numerical simulations based on various samples of a periodic microstructure (Zaoui, 2001; Besson et al., 2001). In that case, the concept of representative volume element (RVE) is often introduced. It represents nowadays an important issue in the mechanics and physics of periodic and random heterogeneous materials with a view to predicting their effective properties. For the French "Institut de Radioprotection et de Sûreté Nucléaire" which is in charge of safety assessment, it is an efficient tool to get quantitative insight into the microstructure of hydrided Zircaloy cladding tubes contained in a nuclear reactor. After some years of life in nuclear reactor, this metal matrix composite exhibits a quasi-brittle behavior which can induce the failure of the cladding tubes during transient loading.

Few works have investigated the existence of an RVE and the possibility to determine its size for random linear heterogeneous materials, notably by using various statistical–numerical analysis. These methods combine numerical simulations (finite elements) with a statistical treatment (multiple realizations for sample generation and statistical analysis of the results). Among them, the methodology of Kanit et al. (2003), constructed within the geostatistical framework (Matheron, 1971), provides a connection between RVE size, number of realizations and estimation accuracy. However, this strategy can be computationally costly — in particular in the case of non-linear behaviors — which potentially reduces its attractiveness for industrial applications. Moreover, it still needs further validations since, so far, it has only been tested for linear mechanical properties (effective elastic and thermal properties). Therefore, this paper intends to develop a new statistical–numerical RVE determination technique that guarantees, for given RVE size and precision, a sufficient number of realizations while offering a good compromise between the RVE size and the total CPU time. This method has also to be flexible enough to be applied to both linear and non-linear properties.

This paper is organized as follows. Section 2 is devoted to an overview of RVE determination techniques. After recalling some classical RVE definitions, we describe the RVE determination approaches of Kanit et al. (2003) and Gitman et al. (2007) that will be useful for the construction of the proposed method. A new statistical–numerical RVE determination technique is introduced in Section 3: the main idea consists in modifying the high CPU cost stabilization technique of Kanit et al. (2003), by introducing a criterion still based on the estimation error but integrating the uncertainty due to the limited size of samples involved in its computation. The test range dealing with a random two-phase quasi-brittle heterogeneous material under dynamic loading, with periodic conditions, is considered in Section 4. This test describes the micromechanical fracture modeling and studies the RVE sensitivity to hydrogen contents. The approach is applied in Section 5 to the RVE size determination of the hydrided Zircaloy with 10% of inclusions. The statistical analysis is first performed for a non-lin-

* Corresponding author. Address: Institut de Radioprotection et de Sûreté Nucléaire, B.P. 3, 13115 Saint-Paul-lez-Durance Cedex, France. Tel.: +33 442 199 617; fax: +33 442 199 166.
E-mail address: yann.monerie@irsn.fr (Y. Monerie).

ear property, the fracture energy, then to linear properties such as apparent stiffness. A correlation factor between linear and non-linear cases is proposed as well. All results are based on intensive numerical simulations performed with the numerical platform XPER (Perales et al., 2008) devoted to the study of dynamic fracture of heterogeneous materials.

2. RVE size determination

The behavior of heterogeneous materials is often described via the concept of representative volume element. Indeed, it is appealing to define the macroscopic structure with the help of a much smaller specimen (that is still large enough to be constitutively valid). Before answering the question of the RVE size for the class of quasi-brittle materials, one needs to properly define the notion of RVE and to summarize the different techniques of the literature in order to find an accurate representative size.

2.1. Review of definitions

Various classes of RVE definition are used in the mechanics of heterogeneous materials.

The first one can be derived from the knowledge of the statistical nature of the microstructure in order to characterize the macroscopic constitutive response of a heterogeneous material. The RVE is usually regarded as a volume V sufficiently large to be statistically representative of the material, i.e. it includes a sampling of all microstructural heterogeneities that occur in the material (Kanit et al., 2003).

The second one is based on statistical properties. The RVE must ensure a given accuracy of the overall estimated properties obtained by spatial averaging of the stress, the strain or the energy fields (Kanit, 2003). This definition, used later in this paper, includes the dependence of the RVE size to the considered mechanical behavior. In particular, it is now clear that the RVE size increases with the non-linearity of the considered behavior (Idiart et al., 2006) and with the *degree of locality* of the studied property: determining a local quantity (e.g. nth order momentum of the strain or stress field) with precision requires a larger RVE than for an overall quantity (e.g. mean strain or stress value).

Another definition given by Drugan and Willis (1996) states that the RVE "is the smallest material volume element of the composite for which the usual spatially constant (overall modulus) macroscopic constitutive representation is a sufficiently accurate model to represent mean constitutive response". This last approach uses the solution of the homogenization for a composite medium and does not consider statistical fluctuations of the effective properties over finite domains.

Several studies have thus been attempted to define an RVE, for different purposes. The review of Gitman et al. (2007) reveals that:

- the RVE should contain enough information on the microstructure (Hashin, 1983);
- the RVE should be sufficiently smaller than the macroscopic structural dimensions (Zaoui, 2001) and sufficiently larger than the microstructural size (Drugan and Willis, 1996);
- the RVE must include a large number of micro-heterogeneities (inclusions, grains, voids, fibers, etc.) (Hill, 1963);
- the statistical homogeneous and ergodic properties ensure that the RVE is statistically representative of the macro response (Ostoja-Starzewski, 1998);
- the response of the RVE must be independent of the boundary condition type (Ostoja-Starzewski, 1998; Sab, 1992);
- the RVE size is given for a specific effective property (Kanit et al., 2003; Gitman et al., 2007) and for a volume fraction of micro-heterogeneities (Gitman et al., 2006; Segurado and Llorca, 2002).

Traditionally, RVE sizes are defined as a minimum size of a microstructural cell that fulfills the requirement of statistic homogeneity. As such, it is a *lower bound*: large microstructural cells behave similarly while smaller microstructural cells do not (Gitman et al., 2006). Ostoja-Starzewski (1998) have noted that the RVE is perfectly defined in two situations: unit cell in a periodic microstructure, and volume containing a very large (mathematically infinite) set of micro-scale elements, possessing statistically homogeneous and ergodic properties.

Concerning the RVE determination in practical cases, two main approaches can be distinguished which are based on:

- experimental observations (Shan and Gokhale, 2002; Romero and Masad, 2004; Graham and Yang, 2003) by combining basic morphological tools (such as covariance or covariogram of a random set (Zaoui, 2001; Jeulin, 2001) with stereological and image analysis techniques in order to describe the geometrical dispersion of the medium;
- effective properties by means of analytical approaches (an explicit non-local constitutive equation is employed (Drugan and Willis, 1996) or numerical analysis (Segurado and Llorca, 2002; Forest et al., 2000; Michel et al., 1999).

From these studies, the differences in the results allow us to conclude that there is a priori no systematic quantification of the RVE sizes (dependence on the material structure, on the volume fraction of heterogeneities, etc.). The numerical estimates of the effective linear properties of random composites seem to be more accurate in the case of small volumes subjected to periodic boundary conditions, if a sufficient number of realizations is considered. These conditions are more suitable than homogeneous strain or stress boundary conditions. By introducing the concept of periodization of random media, Sab and Nedjar (2005) give a new definition of RVE which leads to estimates of its minimum size in agreement with existing theoretical results. They propose a qualitative convergence criterion for the numerical finite element simulations of a two-phase composite. This type of numerical estimates requires a statistical procedure to analyze the results. Among statistical strategies, one can mention: the χ^2 criterion (Gitman et al., 2007), the stochastic stability (Gitman et al., 2006), the stabilization of average and variance (Kanit et al., 2003), a tolerance for the scatter (Vinogradov, 2001), the two-point probability (Zeman and Sejnoha, 2001; Roberts and Garboczi, 2000), etc. Most of them are based on Monte–Carlo simulations (Ostoja-Starzewski, 1998; Gusev, 1997).

In this paper, we focus on a new numerical and statistical approach in the case of volumes with periodic boundary conditions. It exploits the key concept of integral range and is based on a new stopping criterion for sample construction integrating a bootstrap technique to evaluate the accuracy in the estimation of statistical quantities of interest.

2.2. Statistical–numerical RVE determination techniques

Since this study is devoted to RVE size determination for non-linear behaviors, we recall in this section two successful RVE determination techniques: the first one proposed by Kanit et al. (2003) provides a general framework for RVE determination and is the starting point of our approach, but remains for the moment limited to linear behaviors; the second one introduced by Gitman et al. (2007) deals with non-linear mechanical behaviors but is still based on a very small number of realizations that can be not sufficient enough in the case of highly non-linear behaviors such as quasi-brittle fracture. In Section 3, the advantages of both approaches are combined to define a new stopping criterion.

Let us first recall some classical morphological tools that are efficient to describe the microstructural heterogeneities of random media. They are then integrated in the numerical and statistical RVE determination technique proposed in the sequel.

2.2.1. Morphological tools

Among morphological tools, the covariance function and its associated integral range provide a characterization of the geometry of random media. The *covariance function* associated to an ergodic and stationary random medium X and denoted $C(X,\boldsymbol{h})$ is the two-point probability function, i.e. the probability for two points with the separation $\boldsymbol{h}$ to be in the set X:

$$C(X,\boldsymbol{h}) = P(\boldsymbol{x}\in X, \boldsymbol{x}+\boldsymbol{h}\in X). \tag{1}$$

For $\boldsymbol{h}=\boldsymbol{0}$, the covariance, $C(X,\boldsymbol{0})$, is the volume fraction of X. Its asymptotic value, called the *covariance range*, is equal to the square of the volume fraction of X and measures the characteristic length scale of the microstructure. In practice, it can be measured by intercepting the covariance functions (for various orientations in case of anisotropy) and their theoretical asymptotes (equal to the square of the volume fraction). The first local minima of the covariance functions can also be considered if there is no intersection (Jeulin, 2001; Kanit et al., 2006). An example of the hydrided Zircaloy is presented in Figs. 1 and 2, with a volume fraction about 5%: the asymptotic value is represented by dotted line. The covariance ranges are obtained in the circumferential and radial directions: $50\times 3\ \mu m^2$.

The covariance function allows to introduce the *integral range* $\mathscr{A}$ (Matheron, 1971; Jeulin, 2001):

$$\mathscr{A} = \frac{1}{C(X,\boldsymbol{0})-C(X,\boldsymbol{0})^2}\int_{\mathbb{R}^n}(C(X,\boldsymbol{h})-C(X,\boldsymbol{0})^2)\,d\boldsymbol{h} \tag{2}$$

where n is the dimension of the space. Defining effective properties from spatial averages of random fields over a volume V, $\mathscr{A}$ leads to get a quantitative insight into the fluctuations of the average values over different realizations of the real microstructure inside the same volume (and therefore into the precision of the estimation). It is then possible to exhibit a RVE corresponding to the volume V such that a given precision is reached. However, these tools remain limited to RVE determination associated to morphological properties such as volume fraction. Kanit et al. (2003) and Kanit (2003) have thus proposed a methodology integrating these tools in order to extend this RVE determination to any effective property.

2.2.2. Overview of the Kanit et al.'s (2003) methodology for linear properties

For the rest of the paper, $\overline{Z}(V)$ denotes the spatial average of a scalar random field $Z(\boldsymbol{x})$ over a volume V:

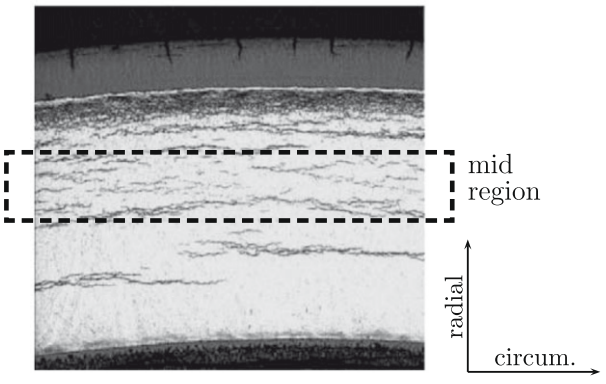

Fig. 1. Microstructure of the hydrided Zircaloy (after Georgenthum et al., 2008). The vertical (resp. horizontal) direction is referred as radial (resp. circumferential) in the sequel.

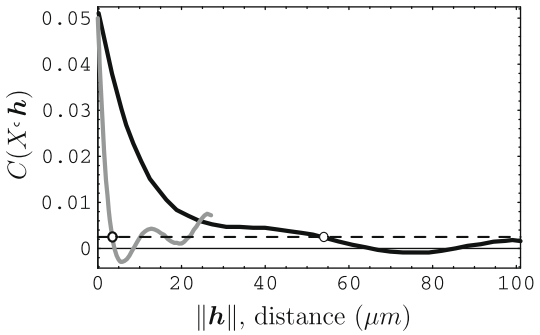

Fig. 2. Circumferential (dark solid line) and radial (gray solid line) covariance functions for the hydrided Zircaloy in the "mid region" (see Fig. 1): volume fraction of inclusions about 5%, theoretical asymptote (dashed line) and covariance ranges (circles).

$$\overline{Z}(V) = \frac{1}{|V|}\int_V Z(\boldsymbol{x})\,d\boldsymbol{x}$$

where $|V|$ is the measure of V. Kanit et al. (2003) introduce the integral range of $Z(\boldsymbol{x})$ as a generalization of Eq. (2) to any random function. For the sake of simplicity in the notations, this quantity is also noted $\mathscr{A}$. The fluctuations of $\overline{Z}(V)$ (or equivalently the variance in statistics) are then expressed thanks to $\mathscr{A}$. More precisely, in the case of an additive scalar over the volume V, the variance of $\overline{Z}(V)$ reads (Matheron, 1971):

$$D_Z^2(V) = D_Z^2\times\left(\frac{\mathscr{A}}{V}\right) \tag{3}$$

where D_Z^2 is the point variance of the random process Z. In case of non-additivity, Kanit et al. (2003) propose the following power law:

$$D_Z^2(V) = D_Z^2\times\left(\frac{\mathscr{A}}{V}\right)^{\alpha} \quad \text{with } \alpha\neq 1. \tag{4}$$

For a two-phase material with linear property Z_1 for phase 1 (with f_v volume fraction) and Z_2 for phase 2 ($1-f_v$ volume fraction), the point variance D_Z^2 is given by:

$$D_Z^2 = f_v(1-f_v)(Z_1-Z_2)^2. \tag{5}$$

Combining (4) and (5), the variance of $\overline{Z}(V)$ is obtained as a function of the volume fraction, the properties of each phase, the volume and the integral range:

$$D_Z^2(V) = f_v(1-f_v)(Z_1-Z_2)^2\left(\frac{\mathscr{A}}{V}\right)^{\alpha}. \tag{6}$$

This variance $D_Z^2(V)$ translates the precision of the estimation of the studied property. Indeed, according to a classical result of sample theory, the absolute error ε_{abs} and the relative error ε_{rel} on the exact mean value M of the random process $\overline{Z}(V)$, obtained with N independent realizations of volume V are deduced from the interval of confidence by:

$$\varepsilon_{abs} = \frac{2D_Z(V)}{\sqrt{N}} \quad \text{and} \quad \varepsilon_{rel} = \frac{\varepsilon_{abs}}{M} = \frac{2D_Z(V)}{M\sqrt{N}}. \tag{7}$$

From (4) and (7), one can derive the number of realizations to reach a given relative error for a fixed volume V by:

$$N = \frac{4D_Z^2(V)}{\varepsilon_{rel}^2M^2} = \frac{4}{\varepsilon_{rel}^2M^2}D_Z^2\left(\frac{\mathscr{A}}{V}\right)^{\alpha}. \tag{8}$$

In the same way, the smallest volume with a given absolute error ε_{abs} and N realizations is:

$$V^{\mathrm{RVE}} = \left(\frac{4}{\varepsilon_{abs}^2N}D_Z^2\right)^{1/\alpha}\mathscr{A}. \tag{9}$$

Algorithm 2.1. Kanit et al.'s (2003) approach can be summarized as follows:

- "generate different realizations of the microstructure for 4–5 different volume sizes V,
- submit each microstructure to loading periodic boundary conditions and record the effective property,
- compute mean value and variance of the effective property for the considered volume sizes; check that the number of realizations was sufficient for each volume by applying the sampling rule (7),
- identify the integral range $\mathscr{A}$ and the power α in model (4),
- set the wanted precision for the estimation of the effective property ε_{rel} and a number of realizations N; use model (9) to deduce the final RVE size".

Eqs. (6), (8) and (9) require to know the true values (or at least an accurate estimation) of the variance $D_Z^2(V)$ and of the exact mean M. In practice, these two quantities are estimated from the available samples for each volume V. More precisely, if $X_N = (\overline{Z}(V)_1, \overline{Z}(V)_2, \ldots, \overline{Z}(V)_N)$ denotes a N-sample associated to volume V, M (resp. $D_Z^2(V)$) is approximated by $M(X_N)$ (resp. $S^2(X_N)$) such that:

$$M(X_N) = \frac{1}{N}\sum_{i=1}^{N} \overline{Z}(V)_i, \quad S^2(X_N) = \frac{1}{N-1}\sum_{i=1}^{N} \left(\overline{Z}(V)_i - M(X_N)\right)^2. \tag{10}$$

Therefore, the accuracy of the estimation strongly depends on the number of realizations chosen by the users. Algorithm 2.1 thus requires a high number of computations (from 10 to 2500, depending on the size of V in Kanit et al. (2003)). The stopping criterion leading to the sufficient number of realizations is based on the stabilization in the estimation of the mean and variance.

This framework is very appealing since the RVE size can be determined for any specific physical or morphological linear property, any given contrast of this property in different phases and any given precision in the estimation. One can find the minimal number or the minimal RVE size by prescribing a RVE size or number, which is not in the initial sampling. Moreover, this procedure can be applied to any microstructure and random model, with different boundary conditions (kinematic uniform, stress uniform and periodic boundaries).

Until now, Kanit et al.'s (2003) approach has provided successful results in the case of a three-dimensional Voronoï mosaic and of a real two-phase heterogeneous material from food industry (Kanit et al., 2006), as for elastic, thermal and morphological properties, like volume fraction. However, the stabilization criterion to select the sufficient number of realizations is computationally costly and not always affordable when considering non-linear properties requiring for each simulation a large number of time steps (plasticity, fracture, etc.). Moreover, to our best of knowledge the ability of the Kanit et al.'s (2003) methodology for non-linear properties has not been tested yet and the connection between elastic and non-linear cases is still an open question. Among recent works dealing with non-linear properties, one can mention the successful works of Gitman et al. (2007) and Gitman (2006), briefly recalled in the sequel.

2.2.3. Overview of Gitman et al.'s (2007) methodology for non-linear properties

In this work, RVE existence and size have been analyzed for three regimes — linear elasticity, hardening and softening — by considering three phase granular materials with various distributions of inclusion size and volume fraction of inclusions. Based on a statistical analysis of numerical experiments (the computed average stress), the authors have concluded about an RVE existence both in the elastic and hardening regimes. In the softening regime, Gitman et al. (2007) seem to conclude to the RVE non-existence. This lack of RVE existence is related to the loss of statistical homogeneity in the material due to the localization of the fracture. To our best of knowledge, the question of the RVE existence is still open and the answer can depend on the overall property of interest and on the type of considered microstructure. Nevertheless, the term "representative" volume element has here to be understood as the domain size over which the proposed statistical–numerical method takes place in order to produce effective fracture energy. The question of the RVE existence for the class of materials we have in mind is further discussed in the last part of the paper.

The Gitman et al.'s (2007) procedure (cf. Algorithm 2.2) uses a χ^2 criterion (11) that measures how the response of a single tested sample deviates relatively from the mean of its class of realizations:

$$\chi^2 = \sum_{i=1}^{N} \frac{\left(\overline{Z}_i(V) - M(X_N)\right)^2}{M(X_N)^2}. \tag{11}$$

Algorithm 2.2. The statistical Gitman et al.'s (2007) process can be summarized as follows:

- "fix the maximum and minimum diameters of inclusions and the initial volume size (usually two times as large as the maximum diameter of inclusions),
- for each given volume fraction of inclusions, generate five realizations (minimal number) of the tested volume size,
- perform the finite element computation and present the numerical results in the form of either load/displacement or stress/strain curve (dependent on the parameter of interest),
- perform the statistical analysis of the obtained finite element results by computing the χ^2 criterion given by (11),
- compare the accuracy[1] of the statistical results with the desired accuracy (usually 95%-accuracy). If the accuracy is good enough, the tested volume size is the RVE size, otherwise increase the volume size and go to the third point".

This statistical process is based on the generation of five samples for each volume fraction and each volume size. In the general non-linear case, such a small number of realizations cannot be sufficient unless considering very large RVE size leading to high computational cost (Kanit et al., 2003).

Therefore, it becomes necessary, for industrial applications, to introduce a new RVE determination technique flexible enough to be applied to both linear and non-linear properties while ensuring a reasonable computational time. Since the geostatistical framework turns out to be appropriate for such a construction, our goal is here to propose a new methodology based on Kanit et al.'s (2003) approach with the following requirements:

- guarantee, for a given RVE size and precision, a minimal number of realizations and offer a good compromise between the RVE size and the CPU time;
- provide a correlation factor between the integral range in the linear and non-linear cases, for the studied material: the hydrided Zircaloy.

[1] Here, accuracy has not the same meaning as within Kanit et al.'s (2003) approach. It is related to a confidence level and not to a relative error. This definition is only considered in this section. For the remaining sections, accuracy is for us similar to precision of the estimation.

3. A new statistical–numerical method

In order to reduce drastically the number of computations required by Kanit's methodology, we start by defining a new stopping criterion.

3.1. Uncertain variance and mean value

As mentioned in the previous section, Eq. (7) plays a central role in the Kanit et al.'s (2003) approach since it connects the precision of the estimation to the integral range thanks to the variance (6). Starting from the same model, the underlying idea of our method is not to consider $D_Z^2(V)$ and M as known value (which requires in Kanit et al. (2003) a large number of computations to reach stabilized variance and mean estimations) but as uncertain parameters. This uncertainty is due to the lack of precision in their estimation because we are working with limited-size samples. In other words, we assume that $D_Z^2(V)$ and M can take any value within an interval range of type $[D^2_{Z,min}(V); D^2_{Z,\max}(V)]$ (resp. $[M_{min}; M_{\max}]$) whose length depends on the number of realizations N.

Integrating uncertainties in (7) for example leads to an uncertainty range associated to the relative error $[\epsilon_{rel,min}; \epsilon_{rel,\max}]$. A stopping criterion can then be defined for each V, as the number of realizations ensuring a narrow uncertainty range (i.e. $\epsilon_{rel,\max} - \epsilon_{rel,min}$) or an upper uncertainty bound ($\epsilon_{rel,\max}$) which does not exceed a given relative error.

The construction of uncertainty ranges for $D_Z^2(V)$ and M and the definition of our stopping criteria are fully detailed in the sequel.

3.1.1. Uncertainty range associated to the mean value M

Similarly to (7), a classical result coming from the theory of sample provides the absolute error related to the estimation of M even if the variance $D_Z^2(V)$ is unknown (Conover, 1999). More precisely, it is possible to derive, using the 95% confidence interval, an uncertainty range for M depending on the sample size N, that reads for each V:

$$I_M = \left[M(X_N) - T_N \frac{S(X_N)}{\sqrt{N}}; \quad M(X_N) + T_N \frac{S(X_N)}{\sqrt{N}} \right] \tag{12}$$

where $M(X_N)$ and $S(X_N)$ are defined by Eq. (10), and where T_N is a value deduced from the 95% confidence interval of the Student law of parameter $N-1$, i.e. $P(-T_N < T \leqslant T_N) = 0.95$, T being the Student law.

Remark 3.1. Similarly to (7), expression (12) is usually established under normality assumption (i.e. when the sample is drawn from a normal probability density function). However, it is still true for any probability density function provided N is sufficiently large.

3.1.2. Uncertainty range associated to the variance $D_Z^2(V)$

Contrarily to the estimation of M, there exists no classical result leading to the uncertainty range associated to $D_Z^2(V)$ without assuming normality. Therefore, a bootstrap technique (Efron and Tibshirani, 1993) is here proposed to exhibit the accuracy of the variance estimation. The computer-based bootstrap method provides measures of accuracy of any statistical estimate. It is performed in three steps (Fig. 3):

- starting from the initial N-sample $X_N = (\overline{Z}(V)_1, \ldots, \overline{Z}(V)_N)$, construct B extra N-samples, $X_N^{(1)}, \ldots, X_N^{(B)}$, drawn with replacement,
- estimate the statistical quantity (i.e. variance) for each sample $((S^2(X_N^{(1)})), \ldots, (S^2(X_N^{(B)})))$,
- estimate the accuracy (i.e. standard error, confidence interval, etc.) of the statistical estimator from the previous sample of variances.

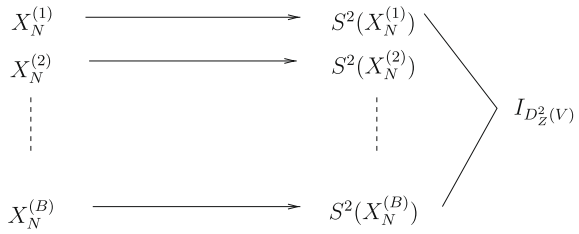

Fig. 3. Sketch of the bootstrap algorithm.

In the following B is set to 1000. Similarly to the mean estimation, we choose the 95% confidence interval to define the uncertainty range, $I_{D_Z^2(V)}$. In practice, it is computed from the empirical cumulative distribution function estimated in the third point of the bootstrap algorithm (the cumulative distribution function of a random variable X is defined by $F_X(x) = P(X \leqslant x)$).

3.1.3. Stopping criterion

After integrating the previous uncertainties and propagating them through Eq. (7), an uncertainty range associated to the relative error can be derived. As can be seen in Fig. 4 and anticipating the results of Section 5, the propagation leads to much more information than an uncertainty range of type $[\epsilon_{rel,min}; \epsilon_{rel,\max}]$. Since the variance and the mean are uncertain, the uncertainty attached to ϵ_{rel} can be summarized by three groups of three curves. From top to bottom, each group corresponds, respectively, to the possible maximal value of the variance (i.e. assuming uncertainty with $D_Z^2(V) = D^2_{Z,\max}(V)$), the variance provided by the estimator (i.e. assuming no uncertainty, $D_Z^2(V) = S^2(X_N)$) and the possible minimal value of the variance (i.e. assuming uncertainty with $D_Z^2(V) = D^2_{Z,min}(V)$). In the same way, the three curves of a same group represent the possible maximal value of the mean, the mean provided by the estimator and the possible minimal value of the mean. Therefore, Fig. 4 appears to be a relevant representation of the available information related to uncertainty. It allows the user to extract the information of interest. Typical strategies can be:

- *Strategy 1*: fix the number of realizations (e.g. $N = 17$) and consider the associated uncertainty range constructed from the uppermost and lowest curves of Fig. 4 (here [1.8%,3.7%]). This strategy is particularly interesting when due to limited computational resources, the number of runs cannot exceed a maximum number of realizations. It is then possible for users to know the uncertainty attached to their results.
- *Strategy 2*: fix the relative error (e.g. $\varepsilon_{rel} = 1.7\%$) and consider the number of realizations to reach this accuracy. From Fig. 4, there are nine possible numbers of realizations. One can then get the expected number following:
  - an "optimistic" strategy that integrates uncertainties but chooses the smallest number of realizations ($N = 22$ with the lowest curve),
  - an "average" strategy that neglects uncertainties and trusts the value given by classical estimators ($N = 36$ with the middle curve of the middle group),
  - a "pessimistic" strategy that focusses on the uppermost curve and leads to the maximal number of realizations ($N = 45$).

The "optimistic" and "average" strategies are less computationally costly than the "pessimistic" one but do not guarantee that the fixed accuracy is reached for this number of realizations. It should be underlined that the Kanit et al.'s (2003) methodology is an "average"-type strategy. In that case the associated lack of

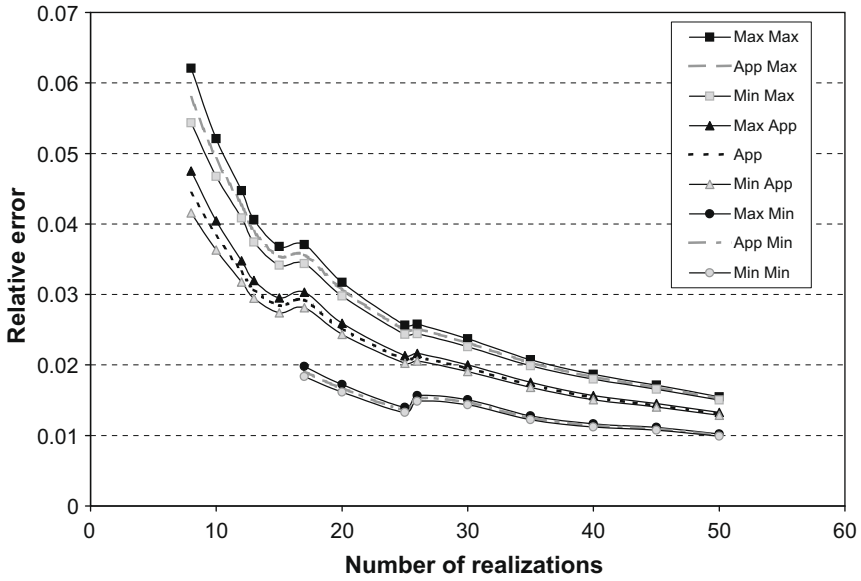

Fig. 4. Example of uncertainty curves associated to the relative error (fracture energy) for a given volume size.

precision is circumvented by performing a very large number of realizations that are not affordable in many non-linear cases.

Keeping in mind that an accurate estimation of the relative error is crucial for RVE determination, we focus on *Strategy 2* for the rest of the paper. By construction, the *"pessimistic" strategy* is the most reliable to ensure an accurate estimation while requiring a lot less simulations than the stabilized procedure associated to the average-type strategies. Therefore, a new stopping criterion is introduced to derive a sufficient number of realizations N such that the relative error in the "worst case" (i.e. provided by the uppermost group of curves), noted for sake of simplicity $\epsilon_{rel,\max}$, does not exceed a given error. The following definition states our new stopping criterion.

Definition 3.1. The sufficient number of computations to reach a relative error of $x\%$ is defined as N_{crit} such that $\epsilon_{rel,\max} \leqslant x\%$.

Based on Fig. 4, the sufficient number of realizations to reach a relative error of 2% is about 37, in our example.

3.2. Statistical–numerical algorithm

Integrating this new stopping criterion, our statistical–numerical method can be summarized as follows:

Algorithm 3.1.

- fix the morphology, the spatial distribution and the volume fraction of the heterogeneities,
- choose various volume sizes,
- *set the desired relative error* and use the new stopping criterion to build a sample for each volume V,
- for each volume V, estimate the variance $D^2_{Z,\max}(V)$,
- taking $D^2_Z(V) = D^2_{Z,\max}(V)$, identify the integral range $\mathscr{A}$ and the coefficient α of the power law (6),
- compute the number of realizations N (if the volume V and the relative error are fixed) or the RVE size (if the number of realizations and the relative error are fixed) using (8) and (9).

In this algorithm the number of realizations is reduced to the minimal number of calculations (according to the selected strategy) required to reach a given accuracy: it is no more necessary to perform a huge number of computer runs to ensure stabilization in the estimations.

Remark 3.2. According to Algorithm 3.1, the integral range is identified once the relative error has been fixed. This procedure reduces drastically the computational cost but the price to pay is that the integral range is estimated with a given accuracy depending on the fixed relative error. This is not completely in full agreement with the geostatistical theoretical framework that assumes that $\mathscr{A}$ does not depend on ϵ_{rel}. However, it is expected that the estimated integral range converges to a stabilized value (i.e. the "true" value of $\mathscr{A}$) for sufficient small relative errors. Therefore, in the numerical applications of Section 5, we fix a small relative error when possible (linear case, Section 5.2). If not, we analyze the evolution of the estimated integral range with respect to the relative error in order to verify its stabilization and to propose a conservative estimation (non-linear case, Section 5.1).

The rest of this paper is devoted to an application of Algorithm 3.1 to the case of two-phase quasi-brittle heterogeneous materials. We start by describing in the next section the test study, focussing on the non-linear property we are interested in. Then, the full analysis is performed for RVE determination of this non-linear property (Section 5) and a connection to the linear case is established as well (by defining the RVE size associated to elastic properties).

4. The test range

This application is related to nuclear fuel safety studies that IRSN is currently conducting. The core of a Pressurized Water Reactor contains a stack of fuel pellets surrounded by a Zircaloy cladding tube. During nuclear reactor operation, the microstructure of these tubes evolves because of the migration/precipitation of hydrogen and the irradiation/oxidation by the water. At high burn-up, this microstructure appears as an heterogeneous two-phase material, constituted of zirconium hydrides inclusions embedded in a Zircaloy metal matrix. The hydride-induced embrittlement can lead to the failure of the fuel rods under accident conditions. The heterogeneities are given by the heterogeneous microstructure (inclusions) and by the cracks in the structure. In order to study the dynamic fracture of this type of non-linear and heterogeneous material, a numerical platform XPER (Perales et al., 2008) has been developed. It especially provides the fracture energy which is the non-linear property we are interested in.

4.1. Fracture modeling and XPER software

The XPER software allows to simulate the fracture dynamics of heterogeneous materials at finite strain, from the crack initiation to non-smooth post-fracture, in a periodic homogenization framework. The micromechanical method developed in Perales et al. (2008) consists in a cohesive/volumetric finite element approach involving the concept of Frictional Cohesive Zone Model (denoted FCZM), in the Non-Smooth Contact Dynamics (NSCD) framework. The effective properties related to fracture mechanics are obtained by periodic numerical homogenization. A two field finite element formulation (including a periodic displacement field and an average deformation gradient field) and an extension of the NSCD method have been introduced (Perales et al., 2008; Perales, 2006).

More precisely, the dynamic fracture is studied using a multibody concept. According to the cohesive/volumetric strategy, the micromechanical modeling consists in introducing FCZM between each element of a finite element mesh:

- the bulk behavior inside the meshes describes the hardening behavior without any damage;
- the FCZM surface properties between the meshes take damage effects into account.

By coupling these both behaviors, the overall progressive damageable behavior is then obtained. The FCZM is a numerical representation of the local physics of the fracture processes, from crack initiation to post-fracture frictional contact on the crack lips. Here, the FCZM is based on the cohesive–friction coupling proposed by Raous et al. (1999) and on an irreversible surface damage law. A cohesive stress $\mathbf{R}^{coh}$ is introduced in the Signorini–Coulomb problem (13) and is related to the displacement jump $[\boldsymbol{u}]$ across the future crack lips:

$$\begin{cases} \widetilde{\boldsymbol{R}} = \boldsymbol{R} + \boldsymbol{R}^{coh}, -\widetilde{R}_N \in \partial I_{\mathbb{R}^+}(u_N), \widetilde{\boldsymbol{R}}_T \in \partial_{\dot{\boldsymbol{u}}_T}(\mu|\widetilde{R}_N|\|\dot{\boldsymbol{u}}_T\|), \\ \boldsymbol{R}^{coh} = \beta\left(C_N \boldsymbol{n}\otimes\boldsymbol{n} + C_T \frac{\boldsymbol{u}_T\otimes\boldsymbol{u}_T}{\|\boldsymbol{u}_T\|^2}\right)\cdot[\boldsymbol{u}]. \end{cases} \tag{13}$$

The subscripts N and T, respectively, denote the normal and the tangential components whereas $\boldsymbol{n}$ is the unit normal vector of the FCZM. C_N and C_T correspond to the initial normal and tangential stiffness of the perfect interface. I_D is the indicator function of the set D and μ the Coulomb friction. The surface variable β of damage is governed by (14) where the function g describes the weakening process leading from perfect interface to crack ($\beta = 1$, the interface is undamaged, $0 < \beta < 1$, the interface is partially damaged and $\beta = 0$, the interface is fully damaged).

$$\begin{cases} \beta = \min(g(\|[\mathbf{u}]\|), g(\|[\mathbf{u}]\|_{\max})), \\ g(x) = \begin{cases} \beta_0 & \text{if} \quad x \leqslant \delta_0, \\ \beta_0 \frac{\delta_0}{x}\left(1 - \left(\frac{x-\delta_0}{\delta_c-\delta_0}\right)^2\right) & \text{if} \quad \delta_0 < x < \delta_c, \\ 0 & \text{if} \quad x \geqslant \delta_c, \end{cases} \end{cases} \tag{14}$$

where $\delta_0 = (R_{\max}/2)(1/C_N + 1/C_T)$, $\delta_c = (3/2)(w/R_{\max} + \delta_0/6)$, $0 \leqslant \beta_0 \leqslant 1$ is an initial surface damage, w is a reference fracture energy, $R_{\max}$ is the maximum value of the cohesive stress and $\|[\mathbf{u}]\|_{\max}$ is the maximum value reached by $\|[\mathbf{u}]\|$ during the fracture process.

Table 1
Bulk material properties.

	Young modulus (GPa)	Poisson's ratio	Yield in tension (MPa)	Hardening modulus (MPa)
Matrix	99	0.325	450	850
Hydride	135	0.32	–	–

The non-regularity introduced by the FCZM relationships (13) and (14) is treated with the NSCD approach (Jean et al., 2001). The dynamic equation combined with contact and friction problems can be written in a discrete form, via an implicit time integration scheme, without any regularization nor penalization.

The determination of the overall behavior of a heterogeneous material is thus numerically made in a multibody *periodic* numerical homogenization framework. The displacement field $\boldsymbol{u}$ is splitted as:

$$\boldsymbol{u} = (\bar{\boldsymbol{F}} - \boldsymbol{I})\cdot\boldsymbol{X} + \boldsymbol{u}^{\#} \tag{15}$$

where $\boldsymbol{X}$ is the initial position vector, $\boldsymbol{I}$ is the second-order identity tensor, $\boldsymbol{u}^{\#}$ is the periodic displacement field and $\bar{\boldsymbol{F}}$ is the mean value of the transformation gradient: $\boldsymbol{F} = \nabla\boldsymbol{u} = \bar{\boldsymbol{F}} + \nabla\boldsymbol{u}^{\#}$. At any boundary of a continuous and independent body K of a finite element discretization, the FCZM (13) and (14) is introduced: $\Pi\cdot\boldsymbol{N} = \boldsymbol{R}([\boldsymbol{u}^{\#}])$, where Π is the first Piola–Kirchhoff stress, $\boldsymbol{N}$ is the outward unit normal vector to K, $[\boldsymbol{u}^{\#}]$ is the periodic part of the displacement jump across ∂K. The NSCD framework is extended to this periodic formulation (Perales et al., 2008).

4.2. Mechanical data

In what follows, the finite element discretization is based on linear displacement triangular elements arranged in a "crossed-triangle" quadrilateral pattern. As can be seen in Fig. 5, the chosen periodic microstructure is composed of a metal matrix (Zircaloy) and randomly distributed rectangular aligned inclusions (zirconium hydrides).

The Zircaloy behavior is assumed to be elastoplastic (von Mises criterion, J2 plasticity) and hydrides to be elastic (see Table 1). The FCZM coefficients of Zircaloy, zirconium hydrides and Zircaloy-hydride interface are given in Table 2. Moreover, a low friction coefficient $\mu = 0.05$ upon the post-crack lips is considered. As indicated in Fig. 5, a macroscopic strain gradient rate is imposed along the direction of the aligned inclusions (direction $\boldsymbol{e}_1$), using the two fields approach (15).

Table 2
Constitutive parameters for cohesive surfaces.

	$C_N = C_T$ (GPa/m)	$R_{\max}$ (MPa)
Matrix/matrix	2×10^9	760
Matrix/hydride	4×10^9	1076
Hydride/hydride	4×10^9	988

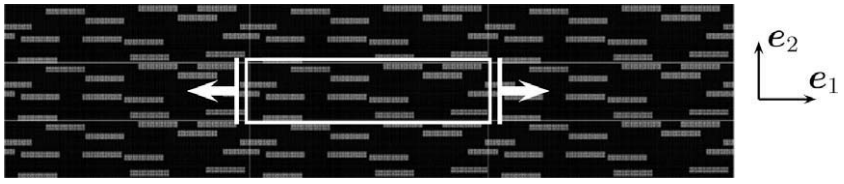

Fig. 5. Illustration of the chosen hydrided Zircaloy microstructure (20% of inclusions) reproduced by periodicity (nine RVEs).

Fig. 6. Example of four realizations for $f_v = 5\%$.

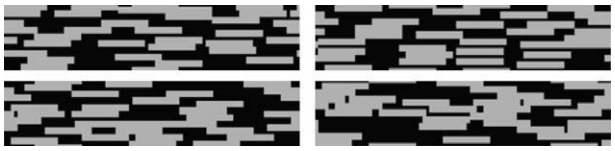

Fig. 7. Example of four realizations for $f_v = 50\%$.

4.3. RVE sensitivity to volume fraction of inclusions

This section is devoted to the study of the effect of the volume fraction on the RVE size and on the fracture energy accuracy. In particular, our attention focusses on the volume fraction of inclusions that gives the maximal standard deviation of the fracture energy. The fracture energy is defined as the strain energy density dissipated during the entire fracture process (area under the stress–strain curve). This sensitivity to volume fraction is performed with a fixed RVE size: a rectangular domain with 20 μm of width and 88 μm of length. The inclusions are also assumed to be rectangular with 2 μm of width and 10 μm of length, and the volume fraction of inclusions f_v varies from 5% to 100%.

Five realizations are considered for each volume fraction of inclusions: five unit cells with the same size but different inclusions distributions are chosen. These distributions are randomly selected according to an initiator system guaranteeing the uniqueness of each realization (Figs. 6 and 7). The centres of inclusions are randomly distributed using a hard-core point process: a non-overlapping distance can be prescribed between each inclusion. This distance is set to zero along the circumferential direction, whatever the volume fraction of inclusions; but is set to one micron along the radial direction for volume fraction lower than 40% and to zero for volume fraction between 40% and 60%. Over 60% of inclusions, a dead leaves process is used in order to reach the prescribed volume fraction of inclusions. This switch could introduce a certain bias in the non-symmetry of the standard deviation of the fracture energy around $f_v = 50\%$. Since the applications we have in mind only concern low volume fraction of inclusions, this bias has no real influence on the results of this study. The hydride-induced embrittlement is underlined in Fig. 8 where stress–strain curves are plotted for volume fraction of inclusions ranging from 0% to 100% (a single initiator for each curve): the maximal stress increases whereas the strain to rupture decreases, when the volume fraction of inclusions increases.

The sensitivity of the overall response to the volume fraction of inclusions is shown in Fig. 9 for volume fraction ranging from 5% to 50%. This figure clearly indicates that the gap between the overall stress–strain curves depends on the volume fraction of inclusions. In particular, looking at the softening part of the curves, this gap increases from $f_v = 5\%$ to $f_v = 10\%$ and decreases from $f_v = 10\%$ to $f_v = 50\%$. A similar tendency is observed in the elastic part of the curves. However, the sensitivity of the overall stress–strain response to the realizations does not seem to be the same in the elastic part and in the softening part. According to these first results (see Fig. 9 for $f_v = 10\%$, top right), it seems that the error range associated to the overall elastic properties is much smaller than the one associated to the fracture energy. This important point, that will be confirmed in the sequel, arises from the fact that the overall elastic properties only depend on the initial microstructure, but that the fracture properties depend over and above on the microstructure induced by the network of developing cracks. Due to localization of the fracture, this induced microstructure takes place at a much larger scale than the one of the initial microstructure. In particular, the final failure is often the consequence of a unique macro-crack.

To conclude this pre-analysis, the sensitivity of relative standard deviation of the fracture energy to the volume fraction of inclusions is given in Fig. 10. The maximal dispersion is about 5% and occurs for $f_v = 10\%$. For the other volume fractions, the dispersion remains smaller than 3%. Therefore, when $f_v = 10\%$, the number of realizations to reach a given accuracy is expected to be larger than the required number associated to the other volume fractions. This value is thus kept for the statistical–numerical computations.

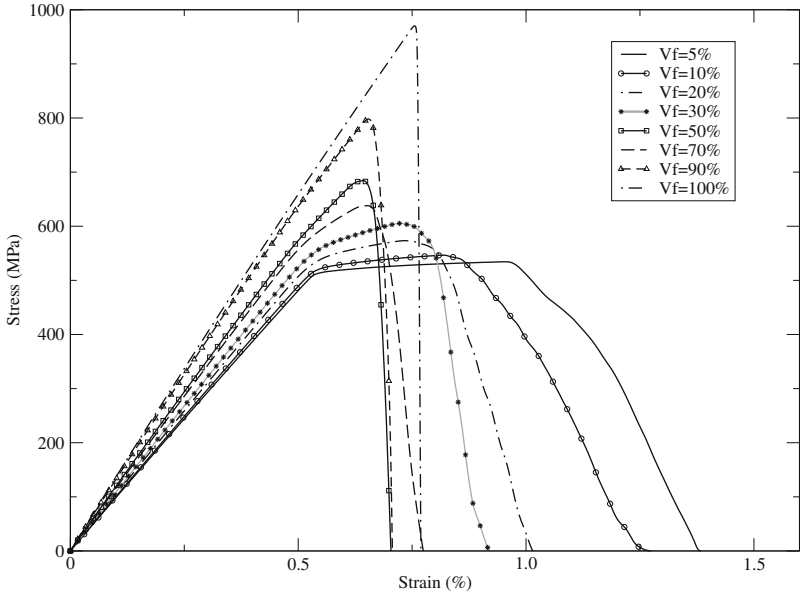

Fig. 8. Overall stress (MPa)–strain (%) curves: one realization per volume fraction.

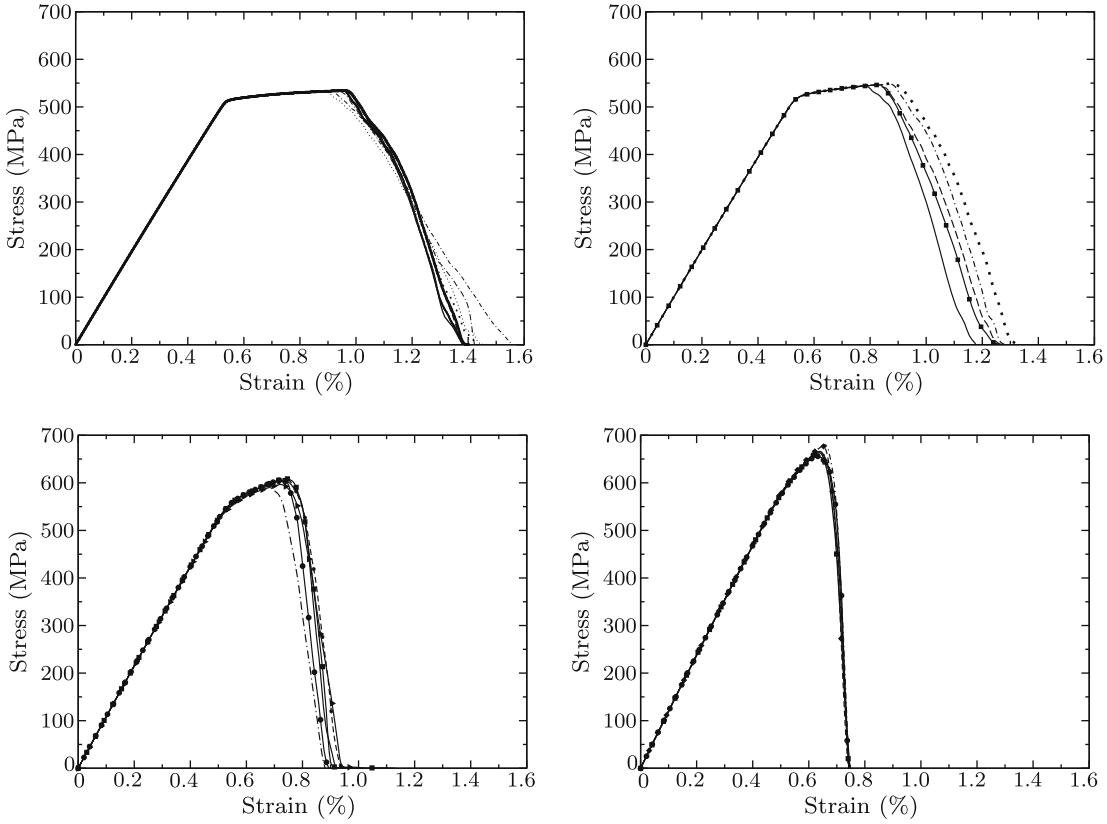

Fig. 9. Overall stress (MPa)–strain (%) curves. Volume fraction of inclusion is from top to bottom, left to right: 5%, 10%, 30%, 50%.

4.4. Determination for each phase of the apparent stiffness and of the fracture energy

In order to use (6)-type statistical expression, the properties Z_i of each phase have to be determined. The properties of interest are here the apparent stiffness, denoted by C_Z (resp. C_H) for the Zircaloy (resp. hydride) phase, and the fracture energy, denoted by E_Z (resp. E_H) for the Zircaloy (resp. hydride) phase.

The stress–strain curves for the Zircaloy without inclusions (Fig. 11 left) and the 100%-hydrided Zircaloy (Fig. 11 right) allow to estimate these properties as:

$$C_Z = 94.99\ \text{GPa} \quad \text{and} \quad C_H = 132.35\ \text{GPa}, \tag{16}$$

$$E_Z = 69.24 \times 10^6\ \text{J/m}^3 \quad \text{and} \quad E_H = 3.86 \times 10^6\ \text{J/m}^3. \tag{17}$$

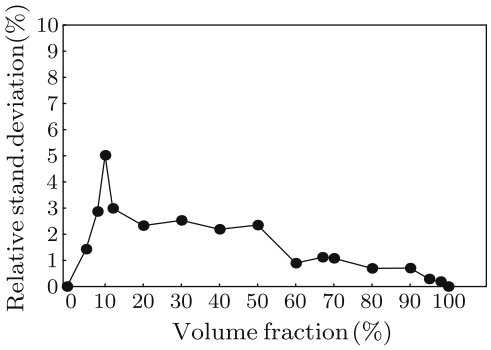

Fig. 10. Relative standard deviation of the overall fracture energy vs volume fraction of inclusions.

5. Numerical results

In this section, our statistical–numerical analysis (Algorithm 3.1) is applied to the previous test study with 10% of inclusions. Keeping in mind the two requirements mentioned at the end of Section 2 (“optimal” non-linear RVE, link between a non-linear RVE and a linear one), we start by focussing on the non-linear property, the fracture energy (denoted E). Then, in order to make the connection to the linear case, we perform the same study for the apparent stiffness (denoted C).

5.1. Fracture energy property

5.1.1. Sample construction

The construction of the samples is based on 13 volume sizes which are listed in Table 3. These volumes have from 2 to 36 inclusions, i.e. their dimension is between 49 μm × 12 μm and 215 μm × 49 μm (RVE aspect ratio is about the same as the inclusions aspect ratio). Fig. 12 displays an example of three periodic volumes. The mean CPU time per volume size is also provided in Table 3: the bigger the volume size, the more important the time calculation (about 5 hours for a RVE with 2 inclusions and about 14 days for a RVE with 36 inclusions). In order to define the number of realizations for all volume sizes, the relative error is arbitrarily set to $\varepsilon_{rel} = 2.5\%$. Following Definition 3.1, we start by plotting, for each volume, the upper uncertainty range ($\epsilon_{rel,\max}$ corresponding to a “pessimistic” strategy) versus the number of realizations (see Fig. 13). It is then straightforward to exhibit the sample size that guarantees a relative error smaller than 2.5%. Note that the curves of Fig. 13 have a monotonous decreasing shape. However, a local non-monotonicity appears around $N = 17$ for the volume corresponding to 10 inclusions and $N = 6$ for the biggest volume. This is due to the fact that the relative error is

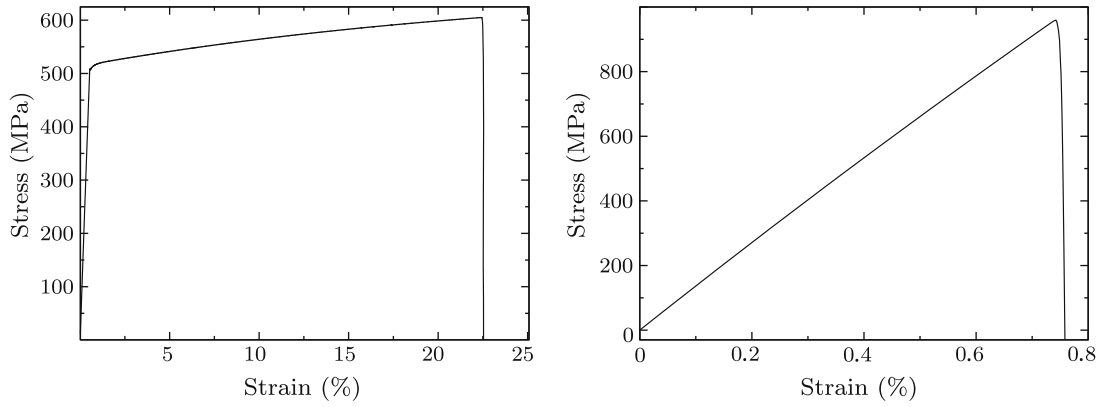

Fig. 11. Overall stress (MPa)–strain (%) curves: (left) Zircaloy matrix, (right) hydride inclusions.

Table 3
Sample size for the fracture energy property: $f_v = 10\%$ and $\varepsilon_{rel} = 2.5\%$.

Number of inclusions	Domain dimensions (μm × μm)	Number of realizations	Max. variance $D^2_{E,\max}(V)$ (10^{12} (J/m^3)^2)	Mean $\overline{E}$ (10^6 J/m^3)	Mean CPU time
2	49 × 12	38	0.105	4.316	4 h 53 min
3	63 × 14	33	0.088	4.245	7 h 12 min
4	69 × 17	25	0.0695	4.220	11 h 13 min
6	88 × 20	19	0.0551	4.299	20 h 10 min
8	102 × 23	15	0.0426	4.380	33 h 19 min
10	113 × 26	12	0.0319	4.436	41 h 52 min
12	126 × 28	13	0.0345	4.416	56 h 45 min
16	138 × 34	10	0.0321	4.424	91 h 12 min
20	163 × 36	8	0.0214	4.380	127 h 32 min
24	176 × 40	6	0.0178	4.385	166 h 37 min
28	191 × 43	6	0.0139	4.312	241 h 51 min
32	204 × 46	5	0.0105	4.360	287 h 42 min
36	215 × 49	6	0.0154	4.345	339 h 49 min

computed using an estimated version of the variance. Therefore, it can happen that, for a given N, a large value of fracture energy is drawn, leading to a larger dispersion. That is why working with the middle group of curves (the "average" strategy) is not satisfactory to derive the number of realizations associated to a prescribed relative error. On the contrary, integrating uncertainty margins in the analysis and considering $\epsilon_{rel,\max}$ guarantees that the fixed relative error is not exceeded.

Table 3 summarizes the number of realizations, the maximal variance and the mean associated to each volume. As expected, the sample size and the variance decrease when the volume size increases.

5.1.2. Estimations of the integral range

The integral range is estimated thanks to (6). From now on the volumes are treated as three dimensional: our simulations were performed in 2D under the plane strain assumption, the length in the third direction being 1 μm. Using Eq. (17), the point variance of the fracture energy property reads:

$$D^2_E = f_v(1-f_v)(E_Z - E_H)^2 \simeq 3.68 \times 10^{14}\ (\mathrm{J/m^3})^2.$$

Since the maximal variance $D^2_{E,\max}(V)$ is known for each volume V, the variance ratio $D^2_{E,\max}(V)/D^2_E$ can be plotted as a function of V (see Fig. 14 left). Taking $D^2_E(V) = D^2_{E,\max}(V)$, a power law of type (4) is then fitted by Least Square Minimization, leading by identification to the integral range $\mathscr{A}_E$ and to the power coefficient α_E. The following values are found:

$$\mathscr{A}_E \simeq 1224\ \mu\mathrm{m}^3 \quad \text{and} \quad \alpha_E \simeq 0.75. \tag{18}$$

Following Remark 3.2, Fig. 14 (right) displays $\mathscr{A}_E$ versus $1/\epsilon_{rel}$. As expected, for small relative error (i.e. large $1/\epsilon_{rel}$) the estimated integral range tends to stabilize. Expression (18) is therefore a

Fig. 12. Example of four periodic volumes, composed of 4, 10 and 20 inclusions, with $f_v = 10\%$.

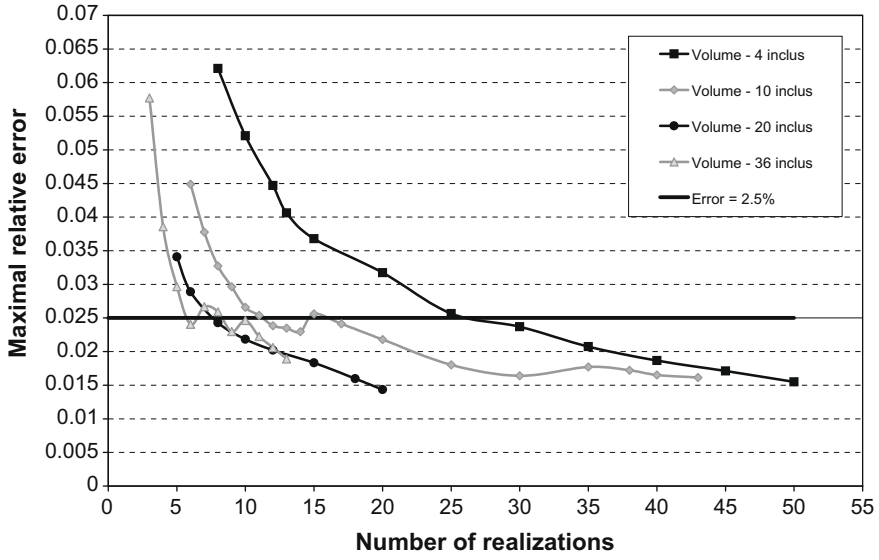

Fig. 13. Application of the stopping criterion: evolution of the maximal relative error for the volumes with, respectively, 4, 10, 20 and 36 inclusions.

conservative estimation of $\mathscr{A}_E$. This last remark will be used later to derive a conservative aspect ratio between the linear and non-linear cases.

The evolution of the number of realizations N is given by (8). It can be written:

$$N = \frac{4}{\varepsilon_{rel}^2 M_E^2} D_E^2 \left(\frac{\mathscr{A}_E}{V}\right)^{\alpha_E} = \kappa_E \left(\frac{\mathscr{A}_E}{V}\right)^{\alpha_E} \tag{19}$$

where κ_E is a constant depending on the studied property. This constant can be evaluated from Eq. (19) and Fig. 15. We get: $\kappa_E \simeq 23.82$.

This result in the non-linear field is very relevant. With a reasonable computer cost, it provides, from the fitted power law and for a given accuracy, the number of realizations (resp. the RVE) for any V (resp. any N) and not only for those of the sample. For example, if the user wants to perform 10 realizations, a volume of 4.4×10^3 µm^3 with 15–16 inclusions is necessary to reach a relative error of 2.5%.

The range of validity of this methodology is illustrated in Fig. 16, where the dispersion and the mean value of the fracture energy associated to the volume samples are plotted. On the left side of this figure, it can be shown that the mean tends to stabilize and that the dispersion decreases when increasing the domain size. Moreover, drawing the relative error $\epsilon_{rel} = 2.5\%$ around the mean value of the fracture energy obtained for the biggest domain, we observed that a convenient precision is attained for domain size over 3000 µm^3, but that more imprecise values can be suspected below this domain size. This situation is clarified on the right side of the figure where this relative error is plotted around the mean value for a small domain size (about 1200 µm^3), an intermediate domain size (about 6000 µm^3) and a large domain size (about 12000 µm^3). For the intermediate and large domain sizes, the relative error range includes the stabilized value of the mean. This is not the case for the small domain size. Performing this analysis of each domain size (not illustrated on the figure) allows to define a domain size below which the methodology is not accurate enough. In the present case, this domain size is about 2000 µm^3.

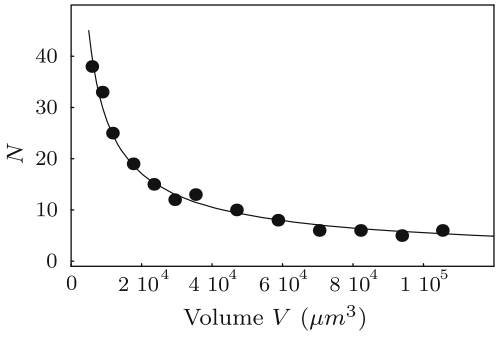

Fig. 15. Fracture energy: number of realizations N as a function of the domain size V for $\varepsilon_{rel} = 2.5\%$: simulations (circle) and model (curve).

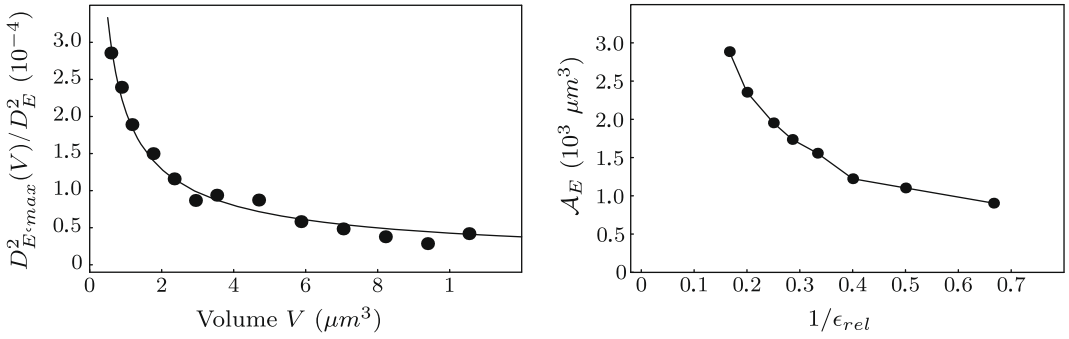

Fig. 14. Left: fracture energy, evolution of the variance ratio as a function of the domain size V; simulations (circle); model (continuous line). Right: evolution of the integral range as a function of the inverse of the relative error.

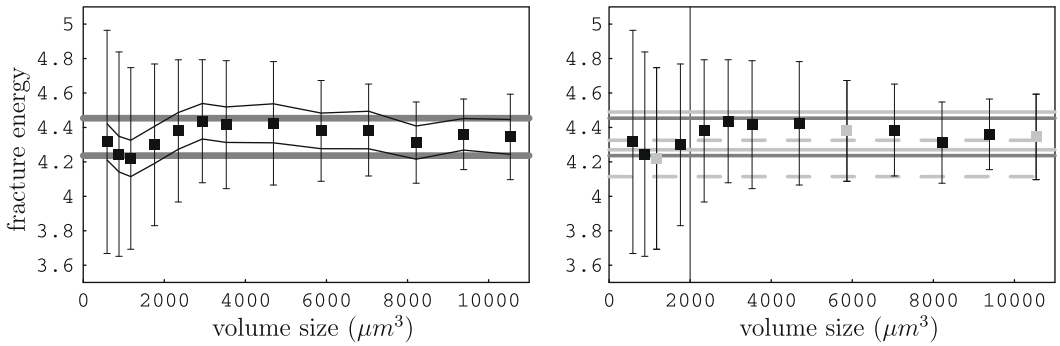

Fig. 16. Mean value ($\bar{E}$) and dispersion ($\pm 2D_E(V)$) of the fracture energy (10^6 J/m^3) as a function of the domain size. Left: relative error $\epsilon_{rel} = 2.5\%$ around the mean value of the fracture energy (thin lines) and focus on the biggest volume (gray thick lines). Right: focus on three domain sizes, a small one (dashed light gray lines), an intermediate one (solid light gray lines) and a large one (solid gray lines). The accuracy of the methodology is ensured for domain sizes over 2000 μm^3.

Note that the mean value of the fracture energy seems to converge when the domain size increases. This situation is not observed by Gitman et al. (2007): the microstructure studied by these authors exhibits a "deterministic size effect" (the probability of the Weibull's "weakest link" increases with respect to the sample size). The microstructure studied here does not seem to exhibit such an effect. This is a priori due to the chosen sampling process used for 10% volume fraction of inclusions: a hard-core point process with non-zero non-overlapping prescribed distance along the direction perpendicular to the macroscopic loading (no creation of cluster of brittle inclusions promoting the mode I fracture). The RVE existence obtained here has thus to be considered as a particular case and no further generic conclusion can be drawn for softening materials.

5.2. Elastic property: apparent stiffness

The statistical–numerical algorithm turns now to be applied to elastic properties. The goal is to identify the model parameters of the power law (6) in order to make the connection between linear and non-linear cases in the next section.

Keeping the same volume sizes for this linear study (see Table 3), Fig. 17 displays the evolution of the maximal relative error (here $\varepsilon_{rel} = 0.01\%$) for some volumes. Note that the obtained value of the relative error is smaller than in the case of the fracture energy; this is in full agreement with comments made in Section 4.3. Elastic properties (16) and (6) give:

$$D_C^2 = f_v(1-f_v)(C_Z - C_H)^2 \simeq 120\ (\text{GPa})^2.$$

From Fig. 18, a power law is fitted using the variance ratio $D^2_{C,\max}(V)/D_C^2$, and the model parameters verify:

$$\mathscr{A}_C \simeq 8.4\ \mu\text{m}^3 \quad \alpha_C \simeq 0.75 \quad \kappa_C \simeq 906.9. \tag{20}$$

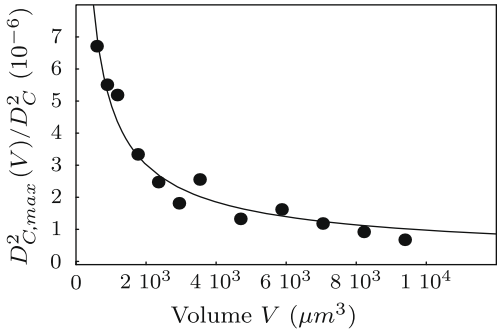

Fig. 18. Apparent stiffness C: evolution of the variance ratio as a function of the domain size V; simulations (circle); model (continuous line).

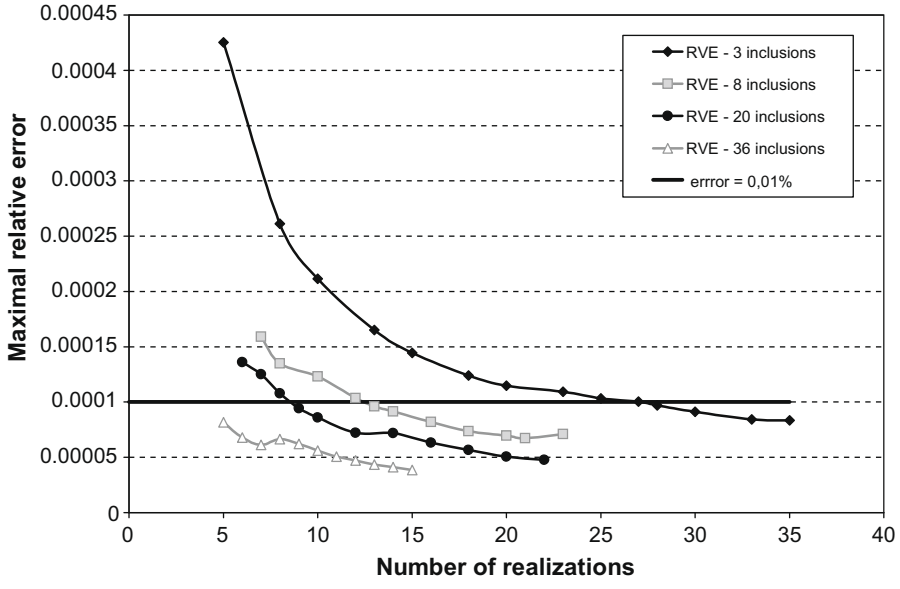

Fig. 17. Application of the stopping criterion: evolution of the maximal relative error of the apparent stiffness C. The RVEs are composed of 3, 8, 20 and 36 inclusions.

Table 4
Comparison of the integral range $\mathscr{A}$ and of the power coefficient α ($f_v = 10\%$) in the linear and non-linear cases.

	Apparent stiffness C	Fracture energy E
ϵ_{rel} (%)	0.01	2.5
Integral range $\mathscr{A}$ (μm^3)	8.4	1224
Power coefficient α	0.75	0.75

Note that the estimated integral range has been derived for a sufficiently small relative error ($\epsilon_{rel} = 0.01\%$) to consider that (20) provides an accurate estimation of the theoretical integral range.

5.3. Towards a connection between linear and non-linear RVE sizes

The goal is here to establish a connection between the RVE characteristics within the linear and the non-linear frameworks. Summarizing the obtained results in Table 4, it appears that the integral range depends on the studied property, for a given volume fraction. The integral range is larger for the non-linear property than for the elastic one. On the contrary, the power coefficient is the same for both properties. This power coefficient is close to one but a bit smaller than the values obtained by Kanit et al. (2003). It is mainly due to the weak values of contrast in the properties of the constituents.

From the present study, we provide the following aspect ratio of *length* in order to connect the linear and the non-linear cases:

$$\sqrt[3]{\frac{\mathscr{A}_E}{\mathscr{A}_C}} \simeq 5.3. \tag{21}$$

As previously mentioned, the obtained value of the integral range for the non-linear property is a conservative estimation of the theoretical value $\mathscr{A}_E$. This estimation is expected to decrease with decreasing relative error until stabilization. Therefore, for sake of reliability, the sensitivity of the aspect ratio to ϵ^E_{rel} has to be studied (Fig. 19) keeping in mind that $\epsilon^C_{rel} = 0.01\%$ is sufficiently small to assume an accurate estimation of $\mathscr{A}_C$ in the linear case. In order to offer the user a good compromise between low computational cost and reliable estimation of integral ranges the aspect ratio is upper bounded according to Fig. 19:

$$\sqrt[3]{\frac{\mathscr{A}_E}{\mathscr{A}_C}} \leqslant 8. \tag{22}$$

This result is valid for the variation range of the relative error that we consider as acceptable and for the volume fraction $f_v = 10\%$. However, since the largest dispersion of the fracture energy corresponds to $f_v = 10\%$ (see Section 4.3), aspect ratio (22) can also be considered as a conservative but reliable connection between RVE characteristics of linear and non-linear cases.

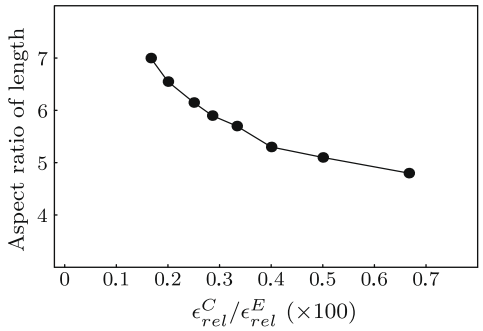

Fig. 19. Evolution of the aspect ratio of length as a function of the ratio of the relative errors.

6. Conclusion

A new statistical–numerical RVE determination method has been developed. This method is based on the classical geostatistical framework previously used in this context by Kanit et al. (2003) and on a new stopping criterion to build the initial samples. This criterion avoids high computational cost that is usually not affordable in many industrial applications or strongly non-linear cases. Its construction relies on: (1) the integration of estimation uncertainty (related to variance and mean) in the identification of the crucial integral range, (2) a sampling strategy that is adapted to the accuracy (i.e. relative error) to reach, reducing the number of realizations (and therefore of computations) to perform for the sample construction.

This methodology has been successfully applied to the RVE determination of a quasi-brittle random metal matrix composites for linear and non-linear properties. The following advantages were pointed out:

- this approach offers a good compromise between an accurate estimation of the RVE size and the required CPU time,
- this approach is flexible enough to be applied to linear and non-linear properties allowing us to exhibit a correlation factor between "linear" and "non-linear" RVEs.

As expected, it came out that the non-linear RVE corresponding to fracture properties is larger than the elastic one. In the case of quasi-brittle fracture properties, the RVE size is found to be about 8–10 times the linear RVE size.

This paper does not analyze the sensibility of this last result to the morphology of the inclusions. This will be done in a forthcoming work.

References

Besson, J., Cailletaud, G., Chaboche, J., Forest, S., 2001. Mécanique non linéaire des matériaux. Hermès Science.

Conover, W., 1999. Practical Nonparametric Statistics. Wiley Series in Probability and Statistics.

Drugan, W., Willis, J., 1996. A micromechanics-based non local constitutive equation and estimates of representative volume element size for elastic composites. J. Mech. Phys. Solids 44 (4), 497–524.

Efron, B., Tibshirani, R., 1993. An Introduction to the Bootstrap No. 57 in Monographs on Statistics and Applied Probability. Chapman & Hall/Crc.

Forest, S., Barbe, F., Cailletaud, G., 2000. Cosserat modelling of size effects in the mechanical behaviour of polycrystals and multi-phase materials. Int. J. Solids Struct. 37, 7105–7126.

Georgenthum, V., Udagawa, Y., Fuketa, T., Desquines, J., 2008. Fracture mechanics approach for failure mode analysis in CABRI and NSRR RIA tests. In: 2008 Water Reactor Fuel Performance Meeting. No. 8070. Seoul, Korea.

Gitman, I., 2006. Representative volumes and multi-scale modelling of quasi-brittle materials. Ph.D. thesis, Delft University of Technology.

Gitman, I., Askes, H., Sluys, L., 2007. Representative volume: existence and size determination. Eng. Fracture Mech. 74, 2518–2534.

Gitman, I., Gitman, M., Askes, H., 2006. Quantification of stochastically stable representative volumes for random heterogeneous materials. Arch. Appl. Mech. 75, 79–92.

Graham, S., Yang, N., 2003. Representative volumes of materials based on microstructural statistics. Scripta Mater. 48, 269–274.

Gusev, A., 1997. A representative volume element size for elastic composites: a numerical study. J. Mech. Phys. Solids 45 (9), 1449–1459.

Hashin, Z., 1983. Analysis of composite materials — a survey. J. Appl. Mech. 50, 481–505.

Hill, R., 1963. Elastic properties of reinforced solids: some theoretical principles. J. Mech. Phys. Solids 11, 357–372.

Idiart, M., Moulinec, H., Ponte Castañeda, P., Suquet, P., 2006. Macroscopic behavior and field fluctuations in viscoplastic composites: second-order estimates versus full-field simulations. J. Mech. Phys. Solids 54 (5), 1029–1063.

Jean, M., Acary, V., Monerie, Y., 2001. Non-smooth contact dynamics approach of cohesive materials. Phil. Trans. R. Soc. Lond. A 359, 2497–2518.

Jeulin, D., 2001. Caractérisation morphologique et modèles de structures aléatoires. In: Bornert, M., Bretheau, T., Gilormini, P. (Eds.), Homogénéisation en mécanique des matériaux, vol. 1. Hermès Science, pp. 95–132 (Chapter 4).

Kanit, T., 2003. Notion of representative volume element for heterogeneous materials: statistical and numerical approach. Ph.D. thesis, Ecole Nationale Supérieure des Mines de Paris.

Kanit, T., Forest, S., Galliet, I., Mounoury, V., Jeulin, D., 2003. Determination of the size of the representative volume element for random composites: statistical and numerical approach. Int. J. Solids Struct. 40, 3647–3679.

Kanit, T., N'Guyen, F., Forest, S., Jeulin, D., Reed, M., Singleton, S., 2006. Apparent and effective physical properties of heterogeneous materials: representativity of samples of two materials from food industry. Comput. Methods Appl. Mech. Eng. 195, 3960–3982.

Matheron, G., 1971. The theory of regionalized variables and its applications. Tech. Rep., Paris School of Mines Publications.

Michel, J., Moulinec, H., Suquet, P., 1999. Effectives properties of composite materials with periodic microstructure: a computational approach. Comput. Methods Appl. Mech. Eng. 172, 109–143.

Ostoja-Starzewski, M., 1998. Random field models of heterogeneous materials. Int. J. Solids Struct. 35, 2429–2455.

Perales, F., 2006. Fissuration des matériaux à gradient de propriétés. application au Zircaloy hydruré. Ph.D. thesis, Université Montpellier II.

Perales, F., Bourgeois, S., Chrysochoos, A., Monerie, Y., 2008. Two field multibody method for periodic homogenization. Eng. Fracture Mech. 75, 3378–3398.

Raous, M., Cangemi, L., Cocu, M., 1999. A consistent model coupling adhesion, friction and unilateral contact. Comput. Methods Appl. Mech. Eng. 177, 383–399.

Roberts, A., Garboczi, E., 2000. Elastic properties of model porous ceramics. J. Am. Ceram. Soc. 83 (12), 3041–3048.

Romero, P., Masad, E., 2004. Relationship between the representative volume element and mechanical properties of asphalt concrete. J. Mater. Civil Eng. 193, 3221–3238.

Sab, K., 1992. On the homogenization and the simulation of random materials. Eur. J. Mech. Solids 11, 585–607.

Sab, K., Nedjar, B., 2005. Periodization of random media and representative volume element size for linear composites. C.R. Mécanique 333, 187–195.

Segurado, J., Llorca, J., 2002. A numerical approximation to the elastic properties of sphere-reinforced composites. J. Mech. Phys. Solids 50, 2107–2121.

Shan, Z., Gokhale, A., 2002. Representative volume element for non-uniform microstructure. Comput. Mater. Sci. 24, 361–379.

Vinogradov, O., 2001. On a representative volume in the micromechanics of particulate composites. Mech. Compos. Mater. 37, 245–250.

Zaoui, A., 2001. Changement d'échelle: motivation et méthodologie. In: Bornert, M., Bretheau, T., Gilormini, P. (Eds.), Homogénéisation en mécanique des matériaux, vol. 1. Hermès Science, pp. 19–39 (Chapter 1).

Zeman, J., Sejnoha, M., 2001. Numerical evaluation of effective elastic properties of graphite fiber tow impregnated by polymer matrix. J. Mech. Phys. Solids 49, 69–90.